

PAPER

# Temporal response of laminated graded-bandgap GaAs-based photocathode with distributed Bragg reflection structure: Model and simulation

To cite this article: Zi-Heng Wang *et al* 2022 *Chinese Phys. B* **31** 098505

View the [article online](#) for updates and enhancements.

## You may also like

- [Near-surface structural study of transition metal oxides to understand their electronic properties](#)  
Yusuke Wakabayashi
- [Graded circular Bragg reflectors: a semi-analytical retrieval of approximate pitch profiles from Mueller-matrix data](#)  
Arturo Mendoza-Galván, Kenneth Järrendahl and Hans Arwin
- [Optimizing the spectro-temporal properties of photon pairs from Bragg-reflection waveguides](#)  
H Chen, K Laiho, B Pressl et al.

# Temporal response of laminated graded-bandgap GaAs-based photocathode with distributed Bragg reflection structure: Model and simulation

Zi-Heng Wang(王自衡)<sup>1</sup>, Yi-Jun Zhang(张益军)<sup>1,†</sup>, Shi-Man Li(李诗曼)<sup>1</sup>, Shan Li(李珊)<sup>1</sup>,  
Jing-Jing Zhan(詹晶晶)<sup>1</sup>, Yun-Sheng Qian(钱芸生)<sup>1</sup>, Feng Shi(石峰)<sup>2,‡</sup>,  
Hong-Chang Cheng(程宏昌)<sup>2</sup>, Gang-Cheng Jiao(焦岗成)<sup>2</sup>, and Yu-Gang Zeng(曾玉刚)<sup>3</sup>

<sup>1</sup> School of Electronic and Optical Engineering, Nanjing University of Science and Technology, Nanjing 210094, China

<sup>2</sup> National Key Laboratory of Science and Technology on Low-Level-Light, Xi'an 710065, China

<sup>3</sup> Changchun Institute of Optics, Fine Mechanics and Physics, Chinese Academy of Sciences, Changchun 130033, China

(Received 10 December 2021; revised manuscript received 15 March 2022; accepted manuscript online 1 April 2022)

To describe the dynamic response characteristics of the laminated graded-bandgap GaAs-based photocathode with distributed Bragg reflection structure, a general theoretical temporal response model is deduced by combining the unsteady continuity equation and numerical calculation method. Through the model, the contribution of the distributed Bragg reflection structure and graded-bandgap emission layer to the temporal response are investigated. Meanwhile, the relationships between the temporal response characteristics of the laminated GaAs-based photocathode and different structural parameters are also analyzed, including average electron decay time, emission layer thickness, and incident light wavelength. It is found that the introduction of distributed Bragg reflection (DBR) layer solves the discrepancy between the absorption capability of the emission layer and the temporal response. Moreover, the distributed Bragg reflection layer can improve the time response by optimizing the initial photoelectron distribution. The improvement effect of the DBR layer on the temporal response is enhanced with the emission layer thickness decreasing or the incident light wavelength increasing. These results explain the effect of the DBR layer of the photocathode on the dynamic characteristics, which can offer a new insight into the dynamic research of GaAs-based photocathode.

**Keywords:** temporal response, GaAs-based photocathode, distributed Bragg reflection, graded-bandgap

**PACS:** 85.60.Ha, 71.55.Eq, 72.10.Bg, 79.60.-I

**DOI:** 10.1088/1674-1056/ac6334

## 1. Introduction

Since the advent of the GaAs-based vacuum photocathode, it has attracted extensive research interest due to its high quantum efficiency, low thermal noise, spin-dependent effects, and high-speed response.<sup>[1–6]</sup> After decades of research, the GaAs-based photocathode gradually becomes irreplaceable in specific application areas, such as night vision imaging, spin-polarized electron source, spectrophotometer, photon counting, laser detection, and thermionic energy converters.<sup>[7–13]</sup> Quantum efficiency is one of the most significant parameters of photocathode. How to improve the quantum efficiency is always a hot issue in numerous photocathode researches. During this period, many approaches regarding structural design have been proposed, such as field-assist structure and distributed Bragg reflection (DBR) structure.<sup>[14–19]</sup> In previous researches, the photoemission process of the photocathode was treated as a steady-state situation for studying quantum efficiency or an unsteady-state situation for investigating temporal response.<sup>[20–23]</sup> For the field-assisted photocathode adopting the varied-doping structure, researchers have explored the temporal response characteristic theoretically and

experimentally.<sup>[24,25]</sup> However, the dynamic temporal properties of the laminated GaAs-based photocathode with DBR structure and graded-bandgap emission layer still lack a suitable model to be described and investigated. Besides, the influence of the DBR structure on the temporal response and the intrinsic mechanism also need to be explained.

According to Spicer's three-step model of photoemission,<sup>[26]</sup> the emission progress of excited electron can be divided into generation, transport and escaping. In the progress of photoelectron generation, the photocathode with graded-bandgap emission layer and DBR reflection layer has different photoelectron generation characteristics and electron transport characteristics. The DBR layer located beneath the emission layer can act as a reflector, which has the function of realizing the total reflection at target wavelength. Hence, the propagating process of the incidence light in the emission layer can be divided into two parts: forward incidence and backward reflection caused by the reflection of DBR structure. In addition, the interface recombination and built-in electric field in the laminated graded-bandgap emission layer also influence the internal transport of photoelectron. Accordingly, this lam-

<sup>†</sup>Corresponding author. E-mail: zhangyijun423@126.com

<sup>‡</sup>Corresponding author. E-mail: shfyf@126.com

inated photocathode requires an appropriate time-dependent photoemission model.

In this paper, a time-dependent photoemission model is deduced to study the temporal response of the laminated GaAs-based photocathode with DBR structure and graded-bandgap emission layer. The derivation method is based on the unsteady one-dimensional continuity equations combined with the numerically discrete calculation. The related optical properties involved in the calculation process are simulated by the finite-difference time-domain (FDTD) method. With the assist of the deduced model, the effect of the secondary absorption caused by the DBR layer and the graded bandgap structure on the temporal response are indicated clearly. We emphatically discuss the effect of DBR structure on the temporal response from the perspectives of emission layer thickness, electron concentration distribution, and incident light wavelength. The analysis results indicate that how the structural design of GaAs-based photocathode influences the temporal response, which will provide effective theoretical guidance for further improvement.

## 2. Structure and theoretical model

The laminated GaAs-based photocathode consists of a DBR layer, a varying-composition, and varying-doping emission layer. As shown in Fig. 1(a), from top to bottom, the photocathode includes a GaAs-based emission layer, a DBR reflection layer, and a substrate. The emission layer is composed of the varying-composition and varying-doping  $\text{In}_x\text{Ga}_{1-x}\text{As}$ . Under the emission layer, the DBR layer is formed by alternately stacking two types of thin materials with different refractive indexes. Through reasonable design, the DBR layer has the function of realizing the total reflection at a specific wavelength. In this case, the original transmission light toward the substrate would be reflected back to the emitting layer, and thus generating the secondary absorption, which improves the absorptivity of the emission layer, especially the absorptivity at the target wavelength.

The energy band structure of the GaAs-based photocathode is shown in Fig. 1(b). Because of the varying-composition and varying-doping structure, the conduction-band  $E_C$  and valence-band  $E_V$  of the emission layer are respectively bent and inclined by the Fermi level leveling effect. Hence, the built-in electric field  $E_{in}$  is generated in the bandgap bending region, and the direction is from the surface toward the bulk. With the assist of the built-in electric field and diffusing effect, the photoelectron transports toward the surface of the emission layer and finally enters into the vacuum. The DBR layer, which is composed of the alternating growing GaAs sublayer and AlAs sublayer, is grown on the high-quality GaAs substrate. The material of DBR structure guarantees the lattice matching at each interface. In addition, the AlAs sublayer

also has the function of preventing the reverse recombination of photoelectron, because of the broad bandgap. In structural design, the emission layer is divided into  $n$  sublayers, and the In composition of each sublayer gradually increases in the direction of electron transport. The doping concentration of the emission layer exponentially decreases in the direction of electron transport.

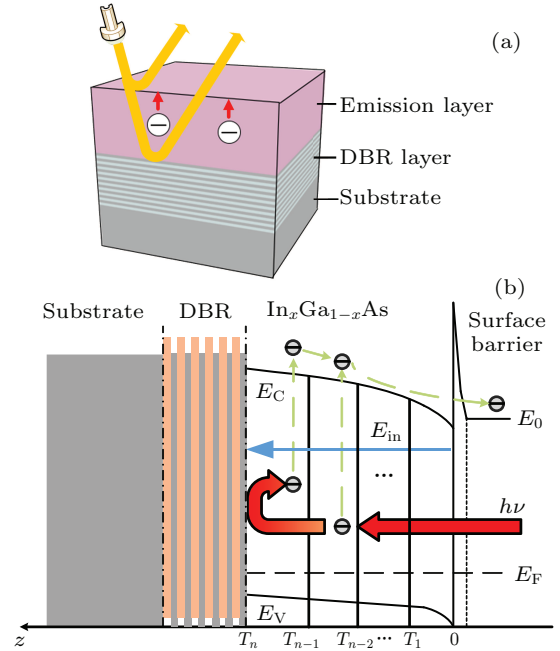


**Fig. 1.** (a) Structure diagram and (b) energy band structure of laminated GaAs-based photocathode, with  $E_C$  being the minimum of conduction band,  $E_V$  the maximum of valence band,  $E_F$  the Fermi level,  $E_0$  the vacuum level, and  $E_{in}$  the built-in electric field.

According to the theory of thin film optics, the thickness of the alternating materials needs satisfy the following expressions to realize the total reflection at target wavelength:

$$\frac{2\pi}{\lambda_{\text{target}}} n_L d_L = \frac{\pi}{2}, \quad (1)$$

$$\frac{2\pi}{\lambda_{\text{target}}} n_H d_H = \frac{\pi}{2}, \quad (2)$$

where  $\lambda_{\text{target}}$  is the target wavelength,  $n_L$  and  $n_H$  are the refractive indices of the materials in the DBR layer respectively, and  $n_H > n_L$ ,  $d_L$  and  $d_H$  are the thicknesses of these two materials in each alternation period. When the In composition changes linearly, the intensity of the built-in electric field generated by the varying-composition and exponential-doping can be calculated by the following formulas:<sup>[14,27,28]</sup>

$$E_1 = \frac{k_0 \cdot T_k}{q_0} \cdot \beta, \quad (3)$$

$$N(0) = N(T_n) \cdot \exp(-\beta \cdot T_n), \quad (4)$$

$$E_2 = \frac{E_{g1} - E_{gn}}{T_n}, \quad (5)$$

$$E_{in} = E_1 + E_2, \quad (6)$$

where  $N(T_n)$  and  $N(0)$  are the doping concentrations at the ends of the emission layer,  $k_0$  is the Boltzmann constant,  $T_k$

the absolute temperature,  $q_0$  the electron charge,  $E_{gn}$  and  $E_{g1}$  are the bandgaps of the innermost sublayer and the outmost sublayer in the emission layer, and  $T_n$  is the total thickness of the emission.

The unsteady one-dimensional continuity equation of the laminated GaAs-based photocathode can be expressed as

$$\frac{\partial n_e(z,t)}{\partial t} = D_{ni} \frac{\partial^2 n_e(z,t)}{\partial z^2} + \mu_i E_{in} \frac{\partial n_e(z,t)}{\partial z} - \frac{n_e(z,t)}{\tau_i} + g(z), \quad i = 1, 2, 3, \dots, n, \quad (7)$$

where  $n_e(z,t)$  is the instantaneous electron concentration in the emission layer,  $D_{ni}$  is the electron diffusion coefficient,  $\mu_i$  is electron mobility,  $\tau_i$  is the lifetime of electron, and the subscript  $i$  value runs from 1 to  $n$ , corresponding to the sublayers with different In compositions in the emission layer. When the incident light transmits through the emission layer at the first time, the light absorption process is called first absorption, and the generation rate of photoelectrons  $g_1(z,t)$  can be expressed as given below. When  $t = 0$ ,

$$g_1(z,0) = \begin{cases} (1 - R_{hv}) I_0 \alpha_{hv1} \exp(-\alpha_{hv1} z), & i = 1, \\ (1 - R_{hv}) I_0 \alpha_{hvi} \left[ \prod_{m=1}^{i-1} \exp(-\alpha_{hvm} d_m) \right] \\ \times \exp[-\alpha_{hvi}(z - T_{i-1})], & i \neq 1; \end{cases} \quad (8)$$

and when  $t \neq 0$ ,

$$g_1(z,t) = 0, \quad (9)$$

where  $R_{hv}$  is the reflectivity of incident surface,  $I_0$  is the intensity of incident light,  $\alpha_{hv}$  is the absorption coefficient,  $d_i$  is the thickness of each sublayer, and  $T_i$  is the position of a sublayer along the  $z$  axis. Because the DBR layer is located behind the emission layer, the transmission part of the incident light will be reflected back into the emission layer and causes the secondary absorption in the emission layer. At this point, the photoelectron generation rate of the secondary absorption can be expressed below. When  $t = 0$ ,

$$g_2(z,0) = \begin{cases} (1 - R'_{hv}) I' \alpha_{hvn} \exp[-\alpha_{hvn}(T_n - z)], & i = n, \\ (1 - R'_{hv}) I' \alpha_{hvi} \left[ \prod_{m=i+1}^n \exp(-\alpha_{hvm} d_m) \right] \\ \times \exp[-\alpha_{hvi}(T_i - z)], & i \neq n, \end{cases} \quad (10)$$

$$I' = I_0 \cdot T_{\text{emission}} \cdot R_{\text{DBR}}; \quad (11)$$

when  $t \neq 0$ ,

$$g_2(z,t) = 0. \quad (12)$$

Then the total photoelectron generation rate  $g(z,t)$  can be obtained from

$$g(z,t) = g_1(z,t) + g_2(z,t), \quad (13)$$

where  $T_{\text{emission}}$  is the transmissivity of the emission layer,  $R_{\text{DBR}}$  is the reflectivity of the DBR layer, and  $R'_{hv}$  is the reflectivity of the emission layer in the backward direction. To solve the differential continuity equation, Eq. (7), the boundary conditions of the interfaces between the sublayers are also necessary, and the equations are given as follows:

when  $i = 2, 3, \dots, n$ ,

$$\left[ D_i \frac{dn_i(z,t)}{dz} + \mu_i |E_{in}| n_i(z,t) \right] \Big|_{z=T_i} = [-S_{v(i+1)} n_i(z,t) + S_{v(i+1)} n_{i+1}(z,t)] \Big|_{z=T_i}, \quad (14)$$

$$\left[ D_i \frac{dn_i(z,t)}{dz} + \mu_i |E_{in}| n_i(z,t) \right] \Big|_{z=T_{i-1}} = S_{vi} n_i(z,t) \Big|_{z=T_{i-1}}, \quad (15)$$

when  $i = 1$ , the boundary condition of the emitting surface can be expressed as<sup>[24]</sup>

$$n(z,t_2) = n(z,t_1) \cdot \exp\left(-\frac{t_2 - t_1}{t_s}\right), \quad (16)$$

where  $t_s$  is the average decay time of the electron concentration at the emitting surface, which is an approximately comprehensive parameter describing the whole photoelectron transport progress,<sup>[24]</sup> and  $S_{vi}$  is the surface recombination rate of each interface. To investigate the time response characteristic of the photocathode, it is assumed that the light source is an ideal pulse source at  $t = 0$ . Hence, the continuity equation, Eq. (7), is given below.

when  $t \neq 0$ ,

$$\frac{\partial n_e(z,t)}{\partial t} = D_{ni} \frac{\partial^2 n_e(z,t)}{\partial z^2} + \mu_i E_{in} \frac{\partial n_e(z,t)}{\partial z} - \frac{n_e(z,t)}{\tau_i}, \quad i = 1, 2, 3, \dots, n; \quad (17)$$

when  $t = 0$

$$n(z,0) = g(z,0), \quad (18)$$

To obtain the dynamic response characteristics, the flux of emitted photoelectrons is expressed as

$$J(t) = -PD_{n1} \frac{\partial n(z,t)}{\partial z} \Big|_{z=0}. \quad (19)$$

Since the exact analytical solution of the unsteady continuity equation cannot be obtained easily through the above equations, the differential discrete method of numerical calculation is utilized to approximate to the actual solution. In this way, the thicknesses of the emission layer and the time lapsing can be discretized into grids. The thickness is divided into  $M$  parts and each spatial step is  $\Delta z$ . The time lapsing is divided into  $K$  parts and each temporal step is  $\Delta t$ . In this case, the electron concentration distribution in the emission layer can be discretized as follows:

$$n(z,t) \Rightarrow n(k\Delta z, j\Delta t) \Rightarrow N_j^k, \quad (20)$$

where  $N$  is the discretized electron concentration distribution,  $j$  is the discretized spatial coordinate,  $k$  is the discretized temporal coordinate. Afterward, the continuity equation and boundary conditions can also be represented by the discretized method. When  $t = 0$ , the initial value of the electron concentration distribution becomes

$$N_j^0 = g(\Delta z \cdot j, 0). \quad (21)$$

It can be found that in the discretized continuity equation, the electron concentration at next temporal step  $N_j^{k+1}$  can be obtained by  $N_{j-1}^k$ ,  $N_j^k$ , and  $N_{j+1}^k$ . Besides, the electron concentration at the interface can be obtained by the boundary conditions. In this case, the discretized electron concentration distribution at different temporal coordinates can be calculated. Eventually, the relationship between the flux of emitted photoelectrons and passed time can be achieved by

$$J(k\Delta t) = -PD_{n1} \frac{N_2^k - N_1^k}{\Delta z}. \quad (22)$$

### 3. Simulation and discussion

The model of the temporal response characteristic of the laminated GaAs-based photocathode is deduced by numerically solving the unsteady one-dimensional continuity equation. In this case, the relationship between the structural design and the temporal response characteristic can be further investigated through the deduced model. The structural parameters of the photocathode are set to be as follows. The  $\text{In}_x\text{Ga}_{1-x}\text{As}$  emission layer is divided into 5 sublayers with different In compositions. The thickness values of sublayers each are 0.1  $\mu\text{m}$ , 0.1  $\mu\text{m}$ , 0.1  $\mu\text{m}$ , 0.1  $\mu\text{m}$ , and 0.7  $\mu\text{m}$ , from bulk to surface, and the In composition values of corresponding sublayers are 0.05, 0.10, 0.15, 0.20, 0.20, respectively. The doping concentration of the entire emission layer exponentially decreases from  $1 \times 10^{19} \text{ cm}^{-3}$  to  $1 \times 10^{18} \text{ cm}^{-3}$ , from bulk to surface. Under the ideal assumption, the In composition in the emission layer increases linearly from 0.05 to 0.20 within a thickness of 0.4  $\mu\text{m}$ . Afterwards, a uniform composition  $\text{In}_{0.2}\text{Ga}_{0.8}\text{As}$  sublayer of 0.7  $\mu\text{m}$  in thickness adjacent to the varying composition sublayers helps to improve the absorption capability at 1064 nm. For computability, it is assumed that the bandgap changes linearly in the varying composition region. In this case, the built-in electric field  $E_2$  generated by the varying composition is considered to be uniform in the varying composition region.<sup>[27,28]</sup> Since the outmost and second sublayers are both  $\text{In}_{0.2}\text{Ga}_{0.8}\text{As}$  material, it is considered that there is no interface between the two sublayers in simulation. Therefore, the photoelectrons in the second sublayer directly travel across the interface into the outmost sublayer without recombination. In simulation, the refractive index and extinction coefficient of GaAs and AlAs are cited from Ref. [29], while the refractive index and extinction coefficient of  $\text{In}_x\text{Ga}_{1-x}\text{As}$  are taken from Ref. [30]. According to Eqs. (1) and (2), to reduce the reflectivity and improve the

photoresponse at 1064 nm, the thickness values of the GaAs and AlAs in the DBR layer are set to be 76 nm and 90 nm, respectively. The quantity cycle of the DBR layer is set to be 10 and the total thickness of the DBR layer is 1.66  $\mu\text{m}$ . Because the propagation time of the incident light in the emission layer and the DBR layer is much less than the temporal response of photocathode, the propagation time is ignored in the simulation. In this case, the optical properties of the photocathode with the mentioned structural design can be simulated to verify the reasonability. As shown in Fig. 2, the FDTD method is utilized to theoretically calculate the reflectivity and the absorptivity spectrum of the photocathode with the above structure. In the process of FDTD simulation, the light source is placed in the vacuum, and the light beam is incident normally on the surface of emission layer. As shown in Fig. 2, the reflectivity curve appears as an oscillating curve in the wavelength range above 800 nm, because of the alternant thin films. According to the theory of DBR design, the lowest wavelength valley when the reflectivity curve fluctuates should be located at 1064 nm. The simulated reflectivity curve and absorptivity curve reach a minimum value and a maximum value at 1064 nm, respectively, which proves that the introduction of DBR structure reliably can improve the absorption capability of emission layer at 1064 nm.

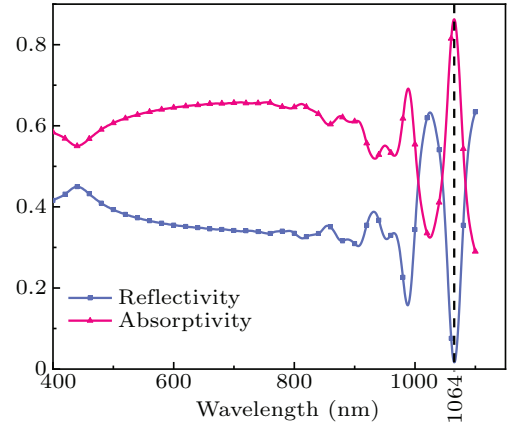


Fig. 2. Simulated reflectivity curve and absorptivity curve of the  $\text{In}_x\text{Ga}_{1-x}\text{As}$  emission layer with DBR structure.

Combining the results of FDTD simulation, the temporal response of the photocathode can be calculated by the deduced model. As for the varying-composition  $\text{In}_x\text{Ga}_{1-x}\text{As}$  emission layer, the band gap, electron mobility, electron diffusion coefficient all depend on In composition  $x$ , and the relationship expressions are given by<sup>[31,32]</sup>

$$E_g(x) = 0.36 + 0.63(1-x) + 0.43(1-x)^2 \text{ (eV)}, \quad (23)$$

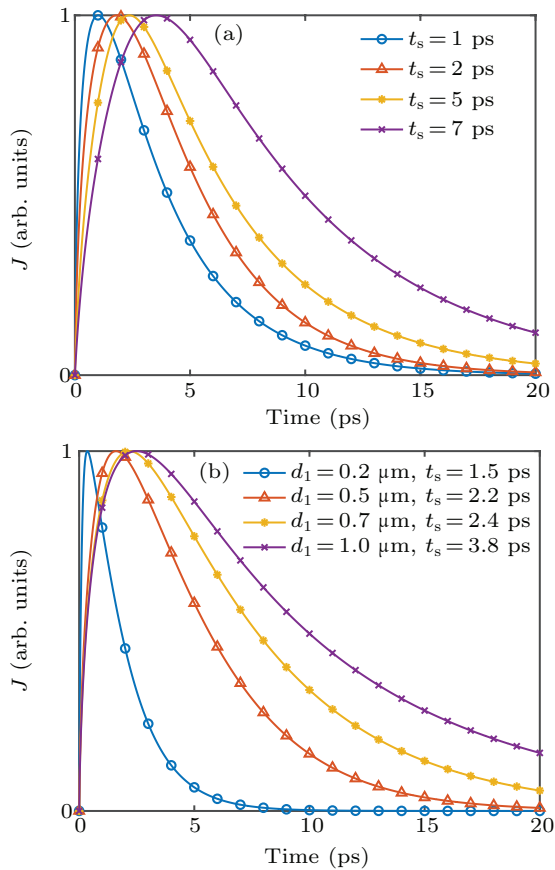
$$\mu(x) = 40 - 80.7(1-x) + 49.2(1-x)^2 \text{ (cm}^2 \cdot \text{V}^{-1} \cdot \text{s}^{-1}\text{)}, \quad (24)$$

$$D(x) = [10 - 20.2(1-x) + 12.3(1-x)^2] \times 100 \text{ (cm}^2 \cdot \text{s}^{-1}\text{)}. \quad (25)$$

The other parameters utilized in the simulation are listed in Table 1 in detail.

**Table 1.** Parameters used in simulation of quantum efficiency curves.

Parameter	Value	Description
$S_{v2}-S_{v5}$	$10^5$ cm/s	electron recombination velocity in emission layer
$P_0$	0.17 <sup>a</sup>	surface electron escape probability
$\alpha_5$ @ 1064 nm	0	absorption coefficient of In <sub>0.05</sub> Ga <sub>0.95</sub> As at 1064 nm
$\alpha_4$ @ 1064 nm	0	absorption coefficient of In <sub>0.10</sub> Ga <sub>0.90</sub> As at 1064 nm
$\alpha_3$ @ 1064 nm	$0.16 \mu\text{m}^{-1\text{b}}$	absorption coefficient of In <sub>0.15</sub> Ga <sub>0.85</sub> As at 1064 nm
$\alpha_1, \alpha_2$ @ 1064 nm	$0.38 \mu\text{m}^{-1\text{b}}$	absorption coefficient of In <sub>0.20</sub> Ga <sub>0.80</sub> As at 1064 nm
$\alpha_5$ @ 960 nm	$0.22 \mu\text{m}^{-1\text{b}}$	absorption coefficient of In <sub>0.05</sub> Ga <sub>0.95</sub> As at 960 nm
$\alpha_4$ @ 960 nm	$0.44 \mu\text{m}^{-1\text{b}}$	absorption coefficient of In <sub>0.10</sub> Ga <sub>0.90</sub> As at 960 nm
$\alpha_3$ @ 960 nm	$0.72 \mu\text{m}^{-1\text{b}}$	absorption coefficient of In <sub>0.15</sub> Ga <sub>0.85</sub> As at 960 nm
$\alpha_1, \alpha_2$ @ 960 nm	$0.99 \mu\text{m}^{-1\text{b}}$	absorption coefficient of In <sub>0.20</sub> Ga <sub>0.80</sub> As at 960 nm
$\alpha_5$ @ 780 nm	$1.97 \mu\text{m}^{-1\text{b}}$	absorption coefficient of In <sub>0.05</sub> Ga <sub>0.95</sub> As at 780 nm
$\alpha_4$ @ 780 nm	$2.49 \mu\text{m}^{-1\text{b}}$	absorption coefficient of In <sub>0.10</sub> Ga <sub>0.90</sub> As at 780 nm
$\alpha_3$ @ 780 nm	$2.60 \mu\text{m}^{-1\text{b}}$	absorption coefficient of In <sub>0.15</sub> Ga <sub>0.85</sub> As at 780 nm
$\alpha_1, \alpha_2$ @ 780 nm	$2.72 \mu\text{m}^{-1\text{b}}$	absorption coefficient of In <sub>0.20</sub> Ga <sub>0.80</sub> As at 780 nm
$\tau_5$	75.36 ps <sup>c</sup>	photoelectron lifetime of In <sub>0.05</sub> Ga <sub>0.95</sub> As
$\tau_4$	67.86 ps <sup>c</sup>	photoelectron lifetime of In <sub>0.10</sub> Ga <sub>0.90</sub> As
$\tau_3$	47.18 ps <sup>c</sup>	photoelectron lifetime of In <sub>0.15</sub> Ga <sub>0.85</sub> As
$\tau_1, \tau_2$	37.38 ps <sup>c</sup>	photoelectron lifetime of In <sub>0.20</sub> Ga <sub>0.80</sub> As

<sup>a</sup>Ref. [33], <sup>b</sup>Ref. [30], <sup>c</sup>Ref. [34]**Fig. 3.** Simulated flux curves of emitted photoelectrons with (a) different surface electron decay time  $t_s$  and (b) different thickness values of uniform composition In<sub>0.2</sub>Ga<sub>0.8</sub>As sublayer.

The flux curves of emitted photoelectron with different values of  $t_s$  are simulated and shown in Fig. 3(a), wherein the total thickness of In<sub>x</sub>Ga<sub>1-x</sub>As emission layer is set to be 1.1  $\mu\text{m}$ . The wavelength of monochromatic pulse light source is 1064 nm. It can be seen obviously that with the

increase of  $t_s$ , the positions of the peak values severely shift to the right and the full widths at half maximum (FWHM) are broadened. According to the definition, in a certain photocathode structure, the value of  $t_s$  should also be determined. Changing the value of  $t_s$  alone can lead to discrepancies in the simulation results as shown in Fig. 2(a). The value of  $t_s$  is relevant to the whole photoelectron transport process, especially the thickness of emission layer. In this case, the value of  $t_s$  is determined by the thickness of emission layer and the relationship is cited from the results of Ref. [24]. The normalized flux curves of emitted photoelectrons with different thicknesses of emission layer are simulated and shown in Fig. 3(b). Because the uniform composition In<sub>0.2</sub>Ga<sub>0.8</sub>As sublayer is the main part of the emission layer, and has the best absorption at 1064 nm, the thickness of the uniform composition In<sub>0.2</sub>Ga<sub>0.8</sub>As sublayer  $d_1$  is adjusted in simulation. It can be seen that the increase of the thickness significantly worsens the temporal response in terms of the right shift of peak and the broadening of FWHM, as shown in Fig. 3(b). With the increase of thickness of the uniform composition sublayer, more photoelectrons are generated in the deeper region, which weakens the enhancement of DBR layer. Besides, the photoelectrons need more transit time to reach the emitting surface.

Although the graded-bandgap emission layer and the DBR layer can improve the quantum efficiency, the effect of this laminated structure on the temporal characteristic still needs further studying. Figure 4(a) demonstrates the normalized flux curves of emitted photoelectrons for the varying composition structure and the uniform composition structure. In the simulations, the total thickness of In<sub>x</sub>Ga<sub>1-x</sub>As emission

layer in the structure with DBR layer is set to be  $1.1\ \mu\text{m}$ . In the comparative structure, the entire emission layer is replaced by a uniform  $\text{In}_{0.2}\text{Ga}_{0.8}\text{As}$  layer with the same thickness. Besides,  $t_s$  is set to be  $2.4\ \text{ps}$  for both structures.<sup>[24]</sup> It can be clearly observed that the photocathode with graded-bandgap emission layer has better temporal response, because the built-in electric field which is opposite to the direction of electron movement, accelerates the movement of electrons. To reduce the influence of structural difference on the result, the temporal response of the proposed structure is simulated without considering the built-in electric field for comparison. The improvement effect of the built-in electric field on the temporal response can be directly observed. According to the above deduced photoelectron generation rate formula, the existence of DBR layer improves the problem of diffusion velocity by the distributing of the generated electrons. Through the above-deduced model of electron concentration distribution, it can be found that the effect of secondary absorption of DBR layer is determined by the thickness of emission layer. Too thick an emission layer will reduce the light energy entering into the DBR layer and weaken secondary absorption. To verify this conjecture, a new photocathode structure with thinner emission layer is simulated for comparison as shown in Fig. 4(b). In this new structure, the total thickness of emission layer is set to be  $0.6\ \mu\text{m}$ , and the thickness of the uniform composition  $\text{In}_{0.2}\text{Ga}_{0.8}\text{As}$  sublayer decreases to  $0.2\ \mu\text{m}$  for reducing the light absorption in the first absorption. Meanwhile, the  $t_s$  is adjusted to  $1.5\ \text{ps}$  due to the decrease of emission layer thickness.<sup>[24]</sup> It can be seen that the improvement effect of the DBR layer on the temporal response becomes more obvious with emission layer thinning, because the proportion of the excited electrons generated by the secondary absorption increases with the thickness of emission layer decreasing.

Figure 5 shows the time evolutions of the electron concentration distribution  $n(z, t)$  in the emission layers with different photocathode structures. The total thickness of the emission layer is set to be  $0.6\ \mu\text{m}$  to emphasize the effect caused by the DBR structure, and  $t_s$  is assumed to be  $1.5\ \text{ps}$ . The emitting surface is located at the origin of abscissa. In Fig. 5(a), it is clear that the initial photoelectron distribution is uniformized by the secondary absorption because of the DBR structure. With the emitting of photoelectron, the electron concentration at the emitting surface decreases rapidly, and a bulge of electron concentration distribution is formed in the bulk as shown in Figs. 5(b)–5(d). In this case, the uniform initial electron concentration distribution can reduce the blocking effect of concentration gradient on photoelectron diffusion. The electron concentration in the  $\text{In}_{0.15}\text{Ga}_{0.85}\text{As}$  sublayer decreases faster, due to a mass of photoelectrons passing through the interface between  $\text{In}_{0.2}\text{Ga}_{0.8}\text{As}$  sublayer and  $\text{In}_{0.15}\text{Ga}_{0.85}\text{As}$

sublayer, and transporting toward the emitting surface. Meanwhile, these figures also demonstrate the characteristics of the DBR layer to enhance the absorption capacity of the emission layer.

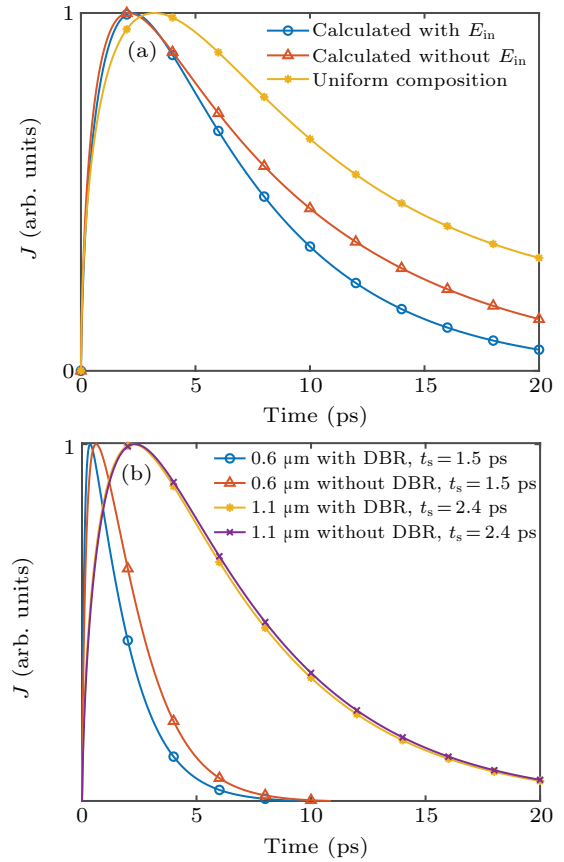


**Fig. 4.** Simulated flux curves of emitted photoelectrons for (a) different built-in electric field cases and (b) different emission layer thickness values with or without DBR layer.

Figure 6 shows the relationship between the DBR structure and temporal response under different incident wavelengths. The total thickness of emission layer is also  $0.6\ \mu\text{m}$  and  $t_s$  is also set to be  $1.5\ \text{ps}$ . It is noted that the improvement effect of DBR structure on the temporal response is obvious for the  $1064\text{-nm}$ -wavelength incident light, while the temporal response of the photocathode with DBR structure is no different from that without DBR structure for the  $780\text{-nm}$ -wavelength incident light. Besides, it can also be found that the improvement effect of DBR structure on the temporal response is reduced when the incident light wavelength decreases. Because the  $\text{InGaAs}$  material has weaker absorption capability for the longer wavelength light, with the wavelength of incident light decreasing, less transmission light can reach the DBR layer and establish the secondary absorption. However, the improvement effect of the DBR structure is determined by the contribution of secondary absorption to total absorption. After the incident light is absorbed completely in the first absorption process, the introduction of DBR layer has no influence on the temporal response.

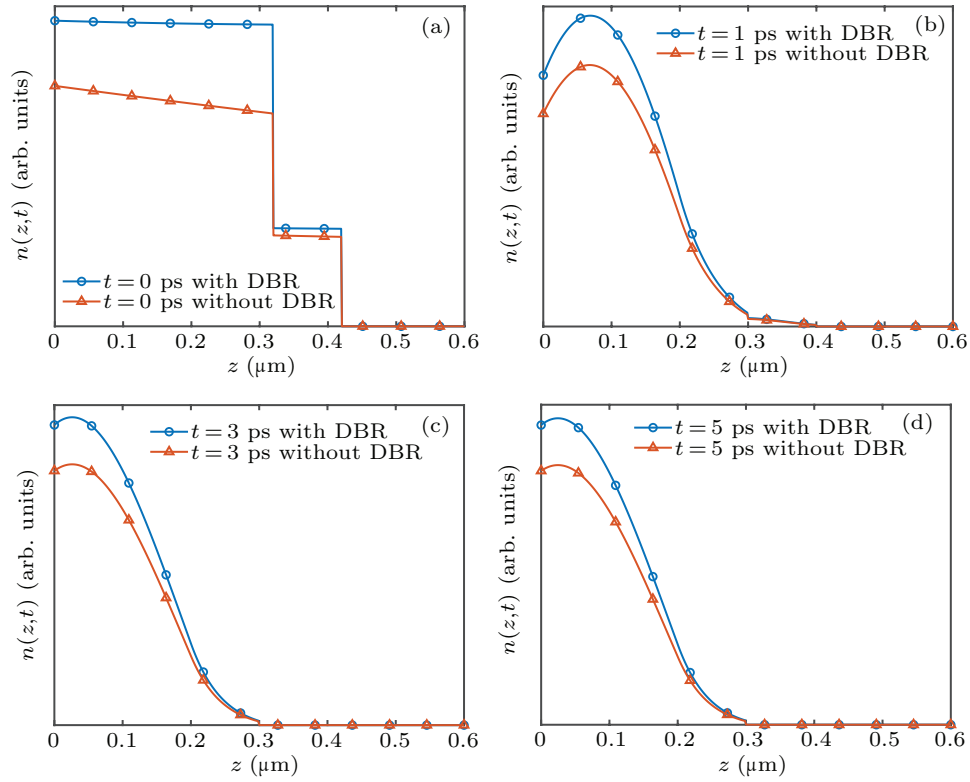


Fig. 5. Electron concentration distributions in emission layer with and without DBR at time  $t = 0$  ps (a), 1 ps (b), 3 ps (c), and 5 ps (d).

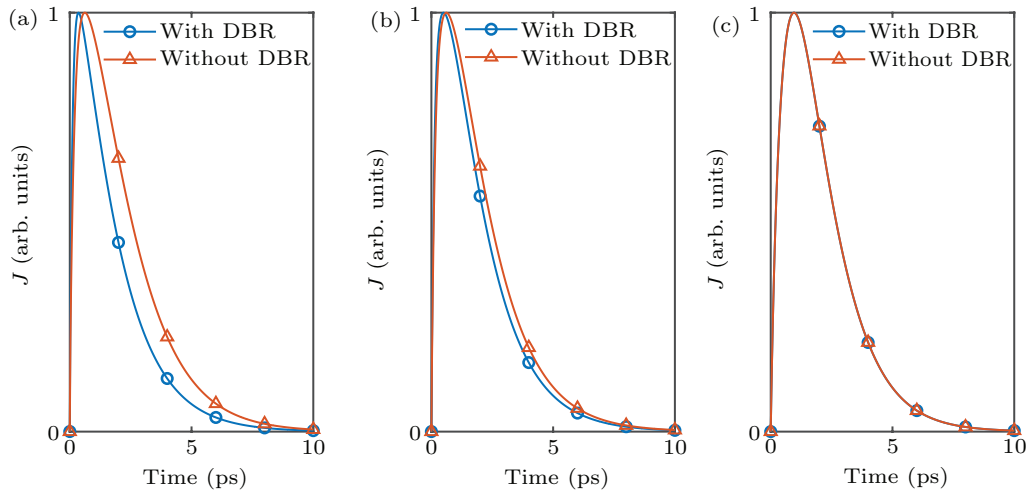


Fig. 6. Simulated flux curves of emitted photoelectrons in emission layer with and without DBR at incident light wavelength of (a) 1064 nm, (b) 960 nm, and (c) 780 nm.

#### 4. Conclusions

In this work, a general theory model is deduced to describe the temporal response of the laminated graded-bandgap GaAs-based photocathode with DBR structure. By solving the unsteady continuity equation through numerical computation method, the time-dependent flux of emitted photoelectrons is obtained. Besides, the relationship between the temporal response and the structural parameters including the thickness of emission layer, the built-in electric field and the DBR structure is explored. Meanwhile, the time evolution of electron concentration distribution in the emission layer and the influence of incident light wavelength on the temporal response are

also simulated. Through the DBR layer, the discrepancy between the absorption capability of the emitting layer and the temporal response can be resolved. By adjusting the initial electron concentration distribution, the temporal response is improved, with the of DBR layer introduced. Moreover, the improvement effect of the DBR layer on the temporal response is enhanced with the decrease of emission layer thickness or the increase of the incident light wavelength. This theoretical model of temporal response characteristic of the complicated GaAs-based photocathode will contribute to the optimization of cathode structure for near infrared response.

## Acknowledgements

Project supported by the National Natural Science Foundation of China (Grant Nos. U2141239 and 61771245) and the Fund from the Science and Technology on Low-Light-Level Night Vision Laboratory of China (Grant No. J20200102).

## References

- [1] Rodionov A A, Golyashov V A, Chistokhin I B, Jaroshevich A S, Derebezov I A, Haisler V A, Shamirzaev T S, Marakhovka I I, Kopotilov A V and Kislykh N V 2017 *Phys. Rev. Appl.* **8** 034026
- [2] Blacksberg J, Maruyama Y, Charbon E and Rossman G R 2011 *Opt. Lett.* **36** 3672
- [3] Schwede J W, Sarmiento T, Narasimhan V K, Rosenthal S J, Riley D C, Schmitt F, Bargatin I, Sahasrabudhe K, Howe R T, Harris J S, Melosh N A and Shen Z X 2013 *Nat. Commun.* **4** 1576
- [4] Rodionov A A, Golyashov V A, Chistokhin I B, Jaroshevich A S, Derebezov I A, Haisler V A, Shamirzaev T S, Marakhovka I I, Kopotilov A V, Kislykh N V, Mironov A V, Aksenov V V and Tereshchenko O E 2017 *Phys. Rev. Appl.* **8** 034026
- [5] Xiao G, Zheng G H, Qiu M, Li Q, Li D S and Ni M J 2017 *Appl. Energy* **208** 1318
- [6] Karkare S, Boulet L, Cultrera L, Dunham B, Liu X H, Schaff W and Bazarov I 2014 *Phys. Rev. Lett.* **112** 097601
- [7] Gallo E M, Chen G N, Currie M, McGuckin T, Prete P, Lovergine N, Nabet B and Spanier J E 2011 *Appl. Phys. Lett.* **98** 241113
- [8] Chen X, Tang G, Wang D and Xu P 2018 *Opt. Mater. Express* **8** 3155
- [9] Suzuno M, Koizumi T and Suemasu T 2009 *Appl. Phys. Lett.* **94** 213509
- [10] Feng C, Zhang Y J, Qian Y S, Wang Z H, Liu J, Chang B K, Shi F and Jiao G C 2018 *Opt. Commun.* **413** 1
- [11] Bae J K, Cultrera L, DiGiacomo P and Bazarov I 2018 *Appl. Phys. Lett.* **112** 154101
- [12] Xuan H, Liu Y A, Qiang P F, Su T, Yang X H, Sheng L Z and Zhao B S 2021 *Chin. Phys. B* **30** 118502
- [13] Karkare S, Boulet L, Cultrera L, Dunham B, Liu X H, Schaff W and Bazarov I 2014 *Phys. Rev. Lett.* **112** 097601
- [14] Feng C, Zhang Y J, Qian Y S, Chang B K, Shi F, Jiao G C and Zou J J 2015 *Opt. Express* **23** 19478
- [15] Zhang Y J, Chang B K, Xiong Y J and Niu J 2011 *Chin. Phys. B* **20** 044209
- [16] Jin M C, Chen X L, Hao G H, Chang B K and Cheng H C 2015 *Appl. Opt.* **54** 8332
- [17] Saka T, Kato T, Nakanishi T, Tsubata M, Kishino K, Horinaka H, Kamiya Y, Okumi S, Takahashi C, Tanimoto Y, Tawada M, Togawa K, Aoyagi H and Nakamura S 1993 *Jpn. J. Appl. Phys.* **32** 1837
- [18] Liu W, Chen Y Q, Lu W T, Moy A, Poelker M, Stutzman M and Zhang S K 2016 *Appl. Phys. Lett.* **109** 252104
- [19] Grobli J C, Oberli D, Meier F, Dommann A, Mamaev Y, Subashiev A and Yashin Y 1995 *Phys. Rev. Lett.* **74** 2106
- [20] Gallo E M, Chen G N, Currie M, McGuckin T, Prete P, Lovergine N, Nabet B and Spanier J E 2011 *Appl. Phys. Lett.* **98** 241113
- [21] Zhou R, Jani H, Zhang Y J, Qian Y S and Duan L Z 2021 *J. Appl. Phys.* **130** 113101
- [22] Bazarov I V, Dunham B M, Li Y L, Liu X H, Ouzounov D G, Sinclair C K, Hannon F and Miyajima T 2008 *J. Appl. Phys.* **103** 054901
- [23] Aleksandrov A V, Avilov M S, Calabrese R, Ciullo G, Dikansky N S, Guidi V, Lamanna G, Lenisa P, Logachov P V, Novokhatsky A V, Tetchio L and Yang B 1995 *Phys. Rev. E* **51** 1449
- [24] Cai Z P, Yang W Z, Tang W D and Hou X 2013 *Mater. Sci. Semicond. Process.* **16** 238
- [25] Honda Y, Matsuba S, Jin X G, Miyajima T, Yamamoto M, Uchiyama T, Kuwahara M and Takeda Y 2013 *Jpn. J. Appl. Phys.* **52** 086401
- [26] Spicer W E 1958 *Phys. Rev.* **112** 114
- [27] Konagai M and Takahashi K 1976 *Solid-State Electron.* **19** 259
- [28] Morales-Acevedo A 2009 *Sol. Energy Mater. Sol. Cells* **93** 41
- [29] Aspnes D E, Kelso S M, Logan R A and Bhat R 1986 *J. Appl. Phys.* **60** 754
- [30] <http://www.ioffe.ru/SVA/NSM/nk/index.html>
- [31] Goldberg Y A and Schmidt N M 1999 *Handbook Series on Semiconductor Parameters*, vol. 2 (London: World Scientific) pp. 62–88
- [32] Goetz K H, Bimberg D, Jurgensen H, Selders J, Solomonov A V, Glinkskii G F and Razeghi M 1983 *J. Appl. Phys.* **54** 4543
- [33] Fisher D G 1974 *IEEE Trans. Electron Dev.* **21** 541
- [34] Fisher D G, Enstrom R E and Williams B F 1971 *Appl. Phys. Lett.* **18** 371